Choppers to optimise the repetition rate multiplication technique on a direct geometry neutron chopper spectrometer

Vickery, Anette; Deen, P. P.

Published in:
Review of Scientific Instruments

Link to article, DOI:
10.1063/1.4900958

Publication date:
2014

Document Version
Publisher's PDF, also known as Version of record

AIP | Review of Scientific Instruments

Choppers to optimise the repetition rate multiplication technique on a direct geometry neutron chopper spectrometer

A. Vickery and P. P. Deen

Citation: Review of Scientific Instruments **85**, 115103 (2014); doi: 10.1063/1.4900958
View online: http://dx.doi.org/10.1063/1.4900958
View Table of Contents: http://scitation.aip.org/content/aip/journal/rsi/85/11?ver=pdfcov
Published by the AIP Publishing

Choppers to optimise the repetition rate multiplication technique on a direct geometry neutron chopper spectrometer

A. Vickery[1,2] and P. P. Deen[2,3]
[1]*DTU Physics, Department of Physics, Fysikvej, building 311, DK-2800 Kgs. Lyngby, Denmark*
[2]*Niels Bohr Institute, University of Copenhagen, Universitetsparken 5, DK-2100 Copenhagen, Denmark*
[3]*European Spallation Source ESS AB, Box 176, 22100 Lund, Sweden*

(Received 2 July 2014; accepted 22 October 2014; published online 10 November 2014)

In recent years the use of repetition rate multiplication (RRM) on direct geometry neutron spectrometers has been established and is the common mode of operation on a growing number of instruments. However, the chopper configurations are not ideally optimised for RRM with a resultant 100 fold flux difference across a broad wavelength band. This paper presents chopper configurations that will produce a relative constant (RC) energy resolution and a relative variable (RV) energy resolution for optimised use of RRM. The RC configuration provides an almost uniform ΔE/E for all incident wavelengths and enables an efficient use of time as the entire dynamic range is probed with equivalent statistics, ideal for single shot measurements of transient phenomena. The RV energy configuration provides an almost uniform opening time at the sample for all incident wavelengths with three orders of magnitude in time resolution probed for a single European Spallation Source (ESS) period, which is ideal to probe complex relaxational behaviour. These two chopper configurations have been simulated for the Versatile Optimal Resolution direct geometry spectrometer, VOR, that will be built at ESS. © *2014 AIP Publishing LLC*. [http://dx.doi.org/10.1063/1.4900958]

I. INTRODUCTION

Direct geometry spectrometers are key workhorse neutron scattering instruments at reactor and spallation source facilities. The scientific fields that commonly employ direct geometry spectrometers are numerous and diverse ranging from magnetism and strongly correlated physics to soft matter and gas storage, to name a few. The strength of direct geometry spectrometers has been fully enhanced with the introduction of position sensitive detectors (PSD) on large area detectors as seen on many of the most recent chopper spectrometers from LET at the ISIS pulsed neutron source[1] to ARCS, SEQUOIA, and CNCS at the Spallation Neutron Source (SNS)[2,3] in Oak Ridge, IN5 at the Institut Laue-Langevin (ILL),[4] 4SEASONS and AMATERAS at J-Parc,[5,6] Neat at HZB,[7] DCS at NIST,[8] Mibemol at LLB,[9] Pelican at ANSTO,[10] and DC-TOF at Kaeri.[11] Four-dimensional S(**Q**, ω) maps are now routine and provide a wealth of information. The next step in accessing broad maps of reciprocal space is through the use of repetition rate multiplication (RRM) that allows one to measure several incident wavelengths within the time period of the source.[12–15] LET, 4SEASONS, and AMATERAS have led the very successful use of RRM on direct geometry spectroscopy instruments.[1,5,6] Nevertheless, the chopper configurations on these instruments are not fully optimised for RRM. The chopper configuration proposed in this paper is fully optimised for RRM with a constant energy resolution, ΔE/E, across the complete wavelength band.

Primarily a direct geometry spectrometer relies on the pulse shaping (PS) and monochromating (M) choppers,[16] choppers 1 and 2, respectively, in Figure 1. A direct geometry spectrometer on a poisoned decoupled moderator of a short pulsed spallation source can employ the time dependence of the source instead of limiting the pulse using a PS chopper. The sketch shows how the primary spectrometer contributions from the M and PS choppers to the energy transfer resolution may be defined geometrically in the case of elastic scattering, i.e., zero energy transfer. The energy transfer resolution for a finite energy transfer is explained in Ref. 17. $\Delta T1$ is the spread of the PS pulse produced at the detector in the case of a hypothetical infinitely sharp opening, in time, of the M chopper. $\Delta T2$ is the spread that an infinitely sharp pulse from the moderator produces at the detector due to the opening time of the M chopper. The opening times of these PS and M choppers, T1 and T2, respectively, are optimised using the principle of balanced resolution, first discussed by Lechner[18] such that the uncertainty of the opening time of the PS chopper, $\Delta T1$, is matched to the uncertainty of the opening time of the M chopper, $\Delta T2$. Balanced resolution ensures optimal flux for a defined energy resolution with the flux at the sample proportional to T1 and T2.

The energy resolution is calculated from the total time uncertainty ΔT_{det} as follows:

$$E = \frac{h^2}{2\,m_n\,\lambda^2} \quad \text{and} \quad \lambda = \frac{h\,T}{m_n\,L_{\mathrm{SD}}}, \tag{1}$$

$$\frac{\Delta E}{E} = \frac{2\,h}{m_n\,L_{\mathrm{SD}}\,\lambda}\,\Delta T_{\mathrm{det}} = \frac{2\Delta T_{det}}{T} = \frac{2\Delta\lambda}{\lambda}, \tag{2}$$

where T is the time of flight for neutrons with wavelength λ from sample to detector with a distance L_{SD}, m_n is the neutron mass, and h is the Planck constant. Figure 1 shows the distances that determine the energy resolution on a chopper spectrometer at a spallation source. L0 is the distance from the moderator to the M chopper. L1 is the distance between the PS and M choppers and L2 is the distance from

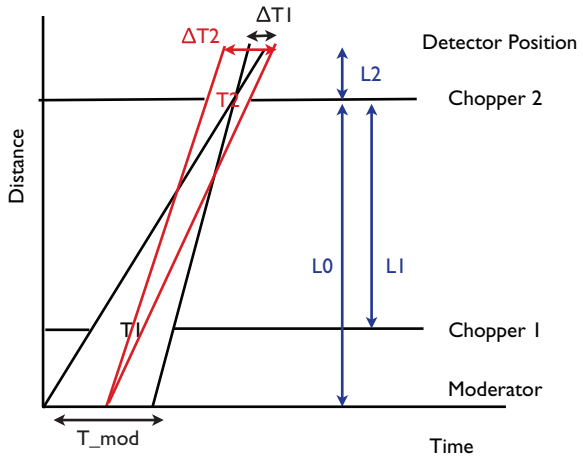

FIG. 1. Time uncertainties and distances on a chopper spectrometer at a spallation source.

the M chopper to the detector position. The opening times are proportional to $\Delta T1$ and $\Delta T2$ in the following manner:

$$\Delta T1 = \frac{L2}{L1} T1; \Delta T2 = \frac{L0 + L2}{L0} T2. \quad (3)$$

The total time uncertainty at the detector, ΔT_{det}, includes, in addition to the contributions $\Delta T1$ and $\Delta T2$ from the primary and secondary spectrometer also a contribution $\Delta T3$ arising from the pathlength uncertainties created by the finite extension of the sample and the detector ΔL_{SD}:

$$\Delta T3 = \frac{m_n \lambda \Delta L_{\text{SD}}}{h}, \quad (4)$$

such that the total time uncertainty of the instrument is defined as

$$\Delta T_{\text{det}} = \sqrt{\Delta T1^2 + \Delta T2^2 + \Delta T3^2}. \quad (5)$$

The opening times of the choppers on current day direct geometry chopper spectrometers do not vary across the time period of the source. However, the relative energy resolution is inversely proportional to the wavelength and the opening time of the choppers. It is therefore clear, from the above equations, that the relative energy resolutions vary substantially across the various incident neutron wavelengths on a wide bandwidth instrument for which the incident wavelengths can vary between by 1 and 9 Å. Equally the flux, proportional to T1 and T2, can vary by up to two orders of magnitude across the wide bandwidth making it impossible to probe transient phenomena simultaneously for all wave vector transfer, S($\mathbf{Q}$, ω).

To realise a wavelength dependent opening time it is possible to use a blind chopper configuration as described in Figure 2. Two choppers, offset by a distance Z, are phased so that chopper I closes as chopper II opens. The nominal wavelength crosses the mean position between choppers I and II. The opening times T_i and T_{i+1}, as shown in Figure 2(a), for adjacent pulses are thus wavelength dependent.

Figure 2(b) shows the analytical opening times of the M chopper required for a range of resolutions and wavelengths and compares these with the calculated opening times provided by the blind chopper. The energy resolutions are al-

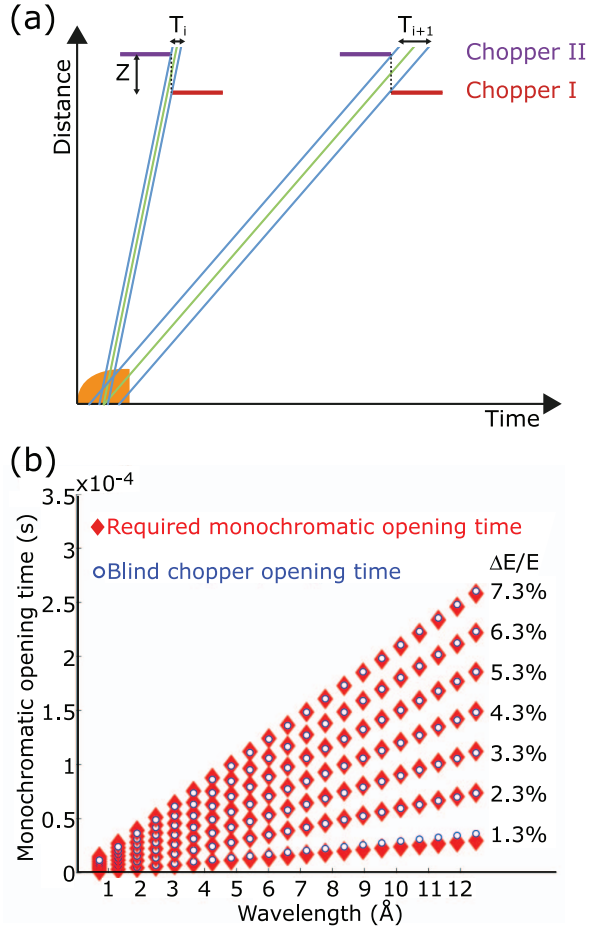

FIG. 2. (a) Diagram outlining the geometric configuration to achieve equivalent energy resolutions for a range of wavelengths. The orange shape represents the moderator pulse structure. (b) Comparison of the M chopper opening times, required for constant energy resolution across a range of wavelengths, with the opening times provided by the blind chopper set-up.

tered by varying the distance Z from $Z = 1.8$ cm for $\Delta E/E = 1.3\%$ up to $Z = 8.4$ cm for $\Delta E/E = 7.3\%$ between the blades of the M chopper. The inter-PS chopper distances required to provide equivalent energy resolutions extends out to 40 cm. We have not decided on the exact mechanism to determine the inter chopper distances. These distances may be adjusted either via translation of the chopper blades or by using a variety of blades positioned at fixed positions. Guide simulations show that a gap in the guide, to allow translation of the blades, results in minimal loss of neutron transmission at the wavelengths and divergences required.[19] The opening times required for a balanced resolution for a given energy resolution across the complete bandwidth can be perfectly provided by the opening times of the blind choppers, see Figure 2(b).

This paper further details a novel chopper configuration for the Versatile Optimal Resolution direct geometry spectrometer, VOR, that can be used in a Relative Constant energy resolution mode (RC) and a Relative Variable energy resolution mode (RV). VOR will be operational at the European Spallation Source (ESS) in 2019.[19] The complete details of the instrument, such as the guide design, are provided elsewhere.[19] Analytical considerations and instrument

simulations of the RV and RC chopper configurations as found on VOR using the ray tracing simulation package McStas version 2.0[20] are detailed in this paper.

II. VOR

VOR provides a broad simultaneous energy coverage for $1 \rightarrow 80+$ meV. Its variable energy resolution, afforded by the long pulse nature of the ESS source and the reduced instrument length, enables increasing the flux quadratically by increasing linearly the energy resolution from $\Delta E/E = 1\%$ up to $\Delta E/E = 6\%$–7%. Focussing the neutron beam onto a $<1 \times 1$ cm^2 beam area optimises the instrument for the study of small, limited lifetime samples and kinetic phenomena. Examples of lifetime limited samples include biological samples that are affected by gamma radiation as produced by the impinging neutrons or samples that are destroyed under a vacuum. The 30.2 m moderator to sample length ensures measurements in the first time frame and avoids parasitic scattering from the prompt pulse over its full dynamic range. Broad momentum space coverage (**Q**) is provided by the angular range of the detector. The characteristics of VOR will be unparalleled in the neutron scattering community and shall provide new insights into novel and exotic phenomena that are currently inaccessible.

The unique time structure of the ESS provides an opportunity to build VOR and provides flux gains per incident wavelength between one and two orders of magnitude in excess of current fluxes on direct geometry chopper spectrometers.[21–23] The incident flightpath on VOR , 30.2 m moderator to sample, is lined with a neutron guide to enhance flux at the sample. The guide, with a rectangular cross section, extends from 2 m to 29.85 m from the moderator and consists of 3 parts: an elliptical shaped guide entry (7.3 m long $m = 5$, the supermirror has a critical angle 5 times that of natural Ni), a 9.3 m long 8 channel bender with radius of curvature 900 m ($m = 2.5$), and an elliptical shaped guide exit (10.7 m long, $m = 2.5$ except the extreme downstream 2.6 m which is $m = 4$) which focus the neutron beam to a $<1 \times 1$ cm^2 beam spot area at the sample position. The incident wavelength bandwidth is defined by the PS and the M chopper systems, centered at 9.5 m and 28.5 m from the moderator and frame overlap is prevented by the RRM chopper at 19 m, a bandwidth chopper at 19.1 m and a set of phased choppers at 28.35 m. Table I provides the information on the dimensions of the choppers and the guide cross sections at the relevant positions. Both the PS, RRM, and M chopper systems are built of counter-rotating chopper pairs (CR), since these represent a better compromise between transmitted intensity and resolution than single blade choppers (SB) rotating at the same speed.[24] We have assumed a separation of 1 cm between the members of a CR. The guide contains appropriate gaps for the chopper systems, 0.4 m for the PS, 0.1 m for the RRM, and 0.15 m for the M, the need for the wide PS and M gaps will be explained in Sec. IV. A 0.1 m long collimation section is positioned between the guide exit and the sample position. The collimation piece is exchangeable and may be inserted to improve divergence profiles. The detector bank is located 3 m from the sample position and has an angular range $-40^\circ < 2\theta < 140^\circ$ and $\pm 26^\circ$, in and out of plane, respectively. A sketch of the instrument layout can be found in Ref. 19.

TABLE I. Chopper and guide parameters. W, H denote the width and height of the guide opening at the chopper position and F denotes the rotation frequency. The radius of the PS and M choppers is 36 cm. CR = counter rotating.

Name	Pos (m)	Type	Slit (deg)	F_{max} (Hz)	W (mm)	H (mm)
PS1	$9.5 - Z_{PS}/2$	CR	40×4	336	38.8	59.4
PS2	$9.5 + Z_{PS}/2$	CR	40×4	336	38.8	59.4
RRM	19	CR	60×4	350	38.8	59.4
BW	19.05	SB	228	14	38.8	59.4
FO	27.5	SB	10	250	27.4	40.0
FO	27.55	SB	10	250	27.4	40.0
M1	$28.5 - Z_M/2$	CR	40×4	336	23.5	30.6
M2	$28.5 + Z_M/2$	CR	40×4	336	23.5	30.6

A. The virtual instrument model

The design of a neutron scattering instrument is strongly based on analytical calculations. However, to fully optimise an instrument geometry and physical performance, for example, with regard to flux, divergence, and resolution, the Monte Carlo ray-tracing simulation packages[25–27] are now proven as versatile tools, both for conceptual design, optimisation and characterization of neutron scattering instruments.[3,28–33] Further, the training of new users, the general planning of experiments and data analysis[34–37] are also areas which benefit from the simulation tools.

The instrument VOR is simulated using the neutron ray-tracing simulation package McStas version 2.0.[20] McStas utilizes a modular approach based on a meta-language specially designed for neutron simulation. The large built-in standard-library of neutron sources, optical elements, and samples, allows the modelling of a complete instrument, component by component. McStas translates automatically the meta-language model into an efficient simulation code in ANSI-C. To account for the ESS moderator pulse length (2.86 ms), the instrument model is based on the `ESS_moderator_long` moderator component with the default parameters. The guide is modelled by 4 components of `Elliptic_guide_gravity` and one bender component `Bender`. The PS and M chopper systems are included in the virtual instrument model, and each of the CR chopper pairs are built of 2 components of `DiskChopper`. The PS choppers are separated by one component of `Guide_gravity`. The collimation section is modelled by `Bender`. The energy resolution at zero energy transfer is simulated with a double-cylinder shaped incoherent scatterer (similar to Vanadium) `Incoherent` at the sample position. The sample thickness is 1 mm and the diameter is 10 mm. The simulated energy resolution is derived from a single time-of-flight sensitive pixel 15×15 mm^2, `TOF_monitor`, in the horizontal scattering plane 3 m from the sample and at $2\theta = 60^\circ$ relative to the incident beam. To enhance statistics, the instrument model applies a 10-fold event repetition (the `SPLIT`

keyword) just before the sample, where random choices of scattering position and scattering direction take place. Further, the sample has the option of focusing onto the detector pixel enabled.

In order to save computing time, simplify the data handling and omit simulating the complete chopper cascade, each RRM pulse is simulated separately. For each pulse the bandwidth of the virtual source is sufficiently wide such that the variance of the time distribution at the detector position is limited by the PS, M chopper systems and the finite extension of the sample. To avoid frame overlap, downstream each chopper system the neutron rays not belonging to the RRM pulse in question are dismissed (`ABSORB`'ed) by a slightly modified version of the `TOF_monitor` component. The complete chopper cascade required to limit frame overlap has been outlined in Ref. 19 and will be published in more detail elsewhere. For each RRM pulse the necessary computing time is inversely proportional to the simulated sample flux, a quantity which for the RC mode varies almost 3 orders of magnitude across the simulated wavelength range (1–9 Å) and energy resolution (2.4%–6.1%). The high resolution vanadium scan at low wavelength ($\Delta E/E \approx 2.4\%$ at $\lambda = 1$ Å) is simulated using 10^{11} neutron rays, while the low resolution at intermediate wavelengths ($\Delta E/E \approx 6.1\%$ at $\lambda = 4$ Å) is simulated using 10^8 neutron rays. For the high resolution mode the simulation of the full instrument is computational heavy and is therefore conducted at the ESS Data Management and Software Centre (DMSC) compute cluster [http://www.ess-dmsc.eu/]. Thus, the computing time ranges from a few seconds to a couple of hours using 30 nodes, each consisting of 2 processors with 6 cores each.

III. CR CHOPPER TRANSMISSION PROFILES

Disk choppers are employed at numerous neutron spectrometers to provide a pulsed neutron beam and thus define the primary spectrometer's contribution to the instrumental energy resolution. As outlined in Sec. I this energy resolution depends on the variances of the time distributions of the neutrons immediately downstream the PS and M choppers and the instrument layout. As detailed by Refs. 24, 38, and 39, the time distribution peak shapes and the variances thereoff may be calculated analytically from the chopper- and guide geometry. Sections V and VI compare the simulated and analytically calculated energy resolutions for the different chopper configurations, RC and RV. This section explains in detail the framework which forms the basis of the analytical calculations.

Figure 3 shows the time distribution of neutrons immediately after passage of a SB and a CR pair of infinitesimally close blades. Both curves have a flat plateau of width $2(\Delta t - \delta t)$ and the base width of the transmission curve is $2(\Delta t + \delta t)$ for a SB and $2\Delta t$ for a CR. These times can be linked to the chopper and guide parameters: chopper frequency F, guide width W, guide height H, chopper blade radius R, and the slit angle ϕ. These parameters are outlined in Figure 3,

$$\Delta t = \frac{1}{2\pi F}\frac{\phi}{2}, \tag{6}$$

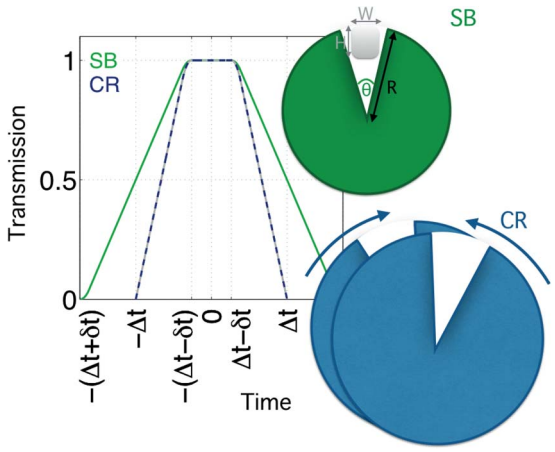

FIG. 3. Calculated transmission curves for a single chopper blade (green full line) and a counter rotating pair of blades with infinitesimal spacing (grey full line). The dashed blue line indicates a linear approximation. The cartoons represent a single (green) and a counter rotating chopper (blue) in front of a neutron guide. The dimensions required to calculate the opening times are provided.

$$\delta t = \frac{1}{2\pi F}\frac{W/2}{R - H}. \tag{7}$$

Clearly, for identical rotation frequencies and chopper/guide geometry, the maximum chopping speed of a CR is twice that of a SB, and in both cases the transmission properties are independent on neutron wavelength and beam divergence. Wavelength dependency is introduced to the transmission curves with a finite separation of the members in a CR. It is demonstrated[38] that a graphical approach is convenient for the derivation of the wavelength dependent transmission curve of a drum chopper. In terms of its transmission properties this device is equivalent to a CR with finite blade separation, provided that effects due to the beam divergence and the shape mismatch between the beam cross section and the slots can be ignored.[39] The diagrams shown in Fig. 4 for the derivation of the CR transmission curve is thus related to the work reported in Refs. 24 and 38. In Fig. 4, the members of the CR are called C1 (upstream) and C2 (downstream) and for simplicity each blade has only one slot. Further it is assumed that the chopper slots undergo a uniform translation with velocity $2\pi(R - H)F$ in the transverse y direction, and that the differential current density of neutrons of wavelength λ in the beam before the first chopper is independent of time and position within the guide. The top panel diagram, which illustrates the simplest case with infinitesimally close members of the CR ($\delta Z = 0$), is included for completeness and is explained first. This diagram shows the lateral position of the chopper slot edges as a function of time relative to the time where the C1 and C2 slots are superposed. In the diagram, a relative phase shift between the blades would correspond to a lateral translation of one pair of parallel lines. The grey area indicates, as a function of time, the lateral extension of the beam. The time that the chopper pair is open to neutrons with lateral coordinate y is $\delta T(y)$ and $P(t)$ is the overall probability for transmission of a neutron arriving at time t at C2. $\delta T(y)$ and $P(t)$ are derived as the width and the height of the grey area, respectively, and $P(t)$, that is the transmission curve, is shown as the black curve at the

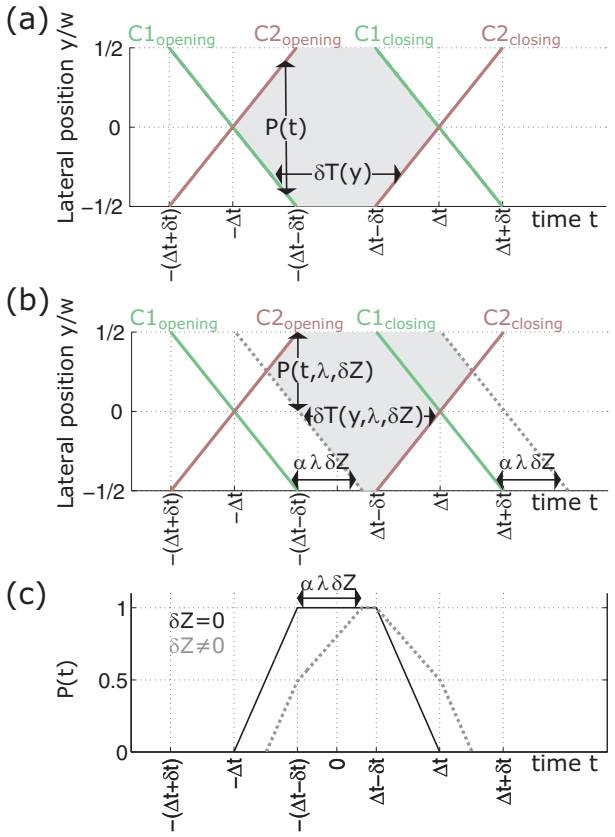

FIG. 4. $\alpha = m_n/h$. Diagrams for illustration of the neutron transmission trough CR with infinitesimal blade separation (top) and finite blade separation δZ along the beam direction (middle). Equation (6) explains the relation of Δt, δt to the chopper parameters outlined in Figure 3. The lower panel shows the transmission curves for the two different cases relative to the time where the chopper slots are superposed.

lower panel. The middle panel illustrates the transmission of neutrons with wavelength λ through a CR with the same phasing as before but with the members separated by the distance δZ parallel to the beam direction. As before, the parallel lines marked C1 represent the lateral position of the C1 slot edges, and the area between these lines indicates the beam lateral extension as a function of time immediately after passage of C1. It takes the neutrons the time $\delta Z\lambda m_n/h$ to travel from C1 to C2. For short blade separation the beam divergence can be ignored, i.e., the beam lateral position is preserved, so immediately before C2 the beam is within the area confined by the parallel dashed lines. On passage of C2 the beam is chopped and the transmission, now dependent on neutron wavelength and blade separation, is defined by $P(t, \lambda, \delta Z)$, $\delta T(y, \lambda, \delta Z)$ found as the height, width of the grey area. As also pointed out in Ref. 39 the relative phasing of the CR members can be changed to compensate for the travel time of neutrons with one particular wavelength. The transmission curve $P(t, \lambda, \delta Z)$ is shown as the dashed grey curve in the lower panel.

IV. THE VOR CHOPPER SYSTEM

The VOR chopper cascade provides two modes of operation: a RC energy resolution mode and a RV energy resolution mode. The RV mode is commonly used on current day direct geometry spectrometers and provides constant chopper opening times for all neutron wavelengths incident at the sample. The RC mode, based on the double blind chopper configuration, provides a constant relative energy resolution, $\Delta E/E$ and thus delivers optimum flux for all incident wavelengths on the sample. The two chopper modes are interchanged by varying the relative frequencies and time offset only.

It should be noted that a full overview of VOR's complete chopper cascade is not provided in this paper. The aim is to provide an overview of the RC and RV chopper configurations. Table I contains a list of the relevant chopper and guide parameters at the chopper positions. The angular opening and maximum frequency of the choppers are chosen to remain within current day technical feasibility. Sections V and VI demonstrate the flexibility of the VOR chopper system to provide a RC or RV energy resolution across a 9 Å wide wavelength band accessed in a single ESS time period. Based on the virtual instrument model described in Sec. II A and the analytically calculated chopper transmission curves outlined in Sec. III, the chopper system is characterized in terms of its peak transmission, relative energy transfer resolution for an energy transfer of zero and the expected sample flux across the 9 Å wide wavelength band. The requirement for RRM is that the frequencies of the PS, RRM, and M choppers must be linked to their relative positions, x:2x:3x with x = 9.5 m on VOR. In addition, the chopper frequencies must be a multiple of the source frequency, 14 Hz. The accessible frequencies are therefore 3×N×14 Hz. The opening times of the M chopper must be able to reach very short opening times and therefore a frequency of 336 Hz has been chosen (336 = 8×3×14 Hz) to remain within conservative technical limits for a 70 cm diameter aluminium disk. Higher speeds can be reached with carbon fiber disks, but the technology is not yet completely proven. As such, the PS choppers can rotate at N×3×14 Hz with N = 2, 3, 4, 6, and 8. A very suitable frequency is 168 Hz that provides 11 pulses through the PS choppers in the ESS source period. An overview of the particular details of opening times across the time period of the ESS is presented in Secs. V and VI.

V. RELATIVE CONSTANT ENERGY RESOLUTION

The RC mode relies on the double blind chopper configuration,[40] a configuration which is commonly employed on neutron time-of-flight reflectometers to provide a broad energy resolution.[41,42] On direct geometry spectrometers opening times of the order of 10 μs are necessary to reach the energy resolutions required by the scientific community. These opening times require great precision, of the order of 100 ns relative to the origin of the ESS pulse. The RC mode double blind chopper configuration employs the closing (PS1, M1) and opening edge (PS2, M2) of the chopper blades to define the time pulses. On VOR it will be important to employ a set of CR chopper blades to provide the necessary sharpness of the closing edge and equally a set of CR chopper blades are required for the sharpness of the opening edge. The requirements for CR blades are further outlined below, in Sec. V A and Sec. V B, where the RC mode transmission profiles, resultant energy resolutions, and flux curves are described. It is

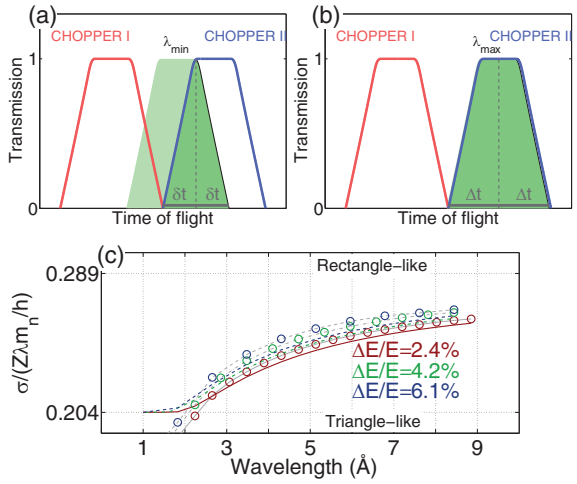

FIG. 5. (a) and (b) The optical blind configuration explained in terms of the chopper transmission curves. The green area is identical to the area under the chopper I transmission (red) curve, but offset in time by $\frac{m_n}{h}\lambda Z$. The resulting (dark green) time pulses correspond to the overlap between the green areas and chopper II (blue) transmission curves. (c) The standard deviation of the time pulse of the PS chopper normalized by the nominal base width of the time pulses. This plot indicates a variation in the peak shapes from triangular to more rectangular with increasing wavelength. Data points are simulated results, the lines are calculated from the guide dimensions, chopper blade geometry and chopper spacing. The chopper blades in the CR pairs are separated by 1 cm.

of interest to understand these profiles since the absolute flux numbers on the sample depend strongly on the beam profile.

Two extreme cases of the transmission through the two sets of choppers of a double blind chopper configuration are exemplified in Figures 5(a) and 5(b). Two CR chopper pairs I and II are separated by the distance Z in the direction of the incident beam. The green area illustrates the transmission of the neutron flux through the first chopper as it reaches the second chopper. The closing edge of the total transmitted pulse, in dark green, is defined by the closing edge of the first chopper. The base width of the transmitted pulse, τ, through both chopper sets is only defined by the time of flight of the neutron beam over the distance Z and is given by $\tau = \frac{m_n}{h}\lambda Z$, provided that $\tau < 2\Delta t$. Figure 5(a) shows that the full peak brightness is only conserved if the pulse half base width is equivalent or exceeds the opening or closing time, δt of the choppers. This means that the minimum energy resolution is determined by δt, and therefore the chopper frequency for a given guide cross section. Figure 5(b) shows that the maximum pulse base width is limited by $2\Delta t$, so that the maximum energy resolution is limited by the chopper frequency for a fixed slit angle. In the case of VOR, the instrument is optimised for high flux on small samples with particular emphasis on transient phenomena. The instrument must be able to trade energy resolution for flux up to 6%–7% for which a triangular slit angle of 40° has been chosen for both the PS and M chopper blades. It may be possible to further optimise the transmission using a rectangular opening slot.

A comparison of panels (a) and (b) in Figure 5 illustrates that the trapezoidal shape of the time pulse through the double blind choppers shows great variation across the bandwidth from λ_{min} to λ_{max}. At the lowest wavelengths and highest energy resolutions a triangular time pulse shape is observed while a more rectangular time pulse shape is approached for the transmission of the highest wavelengths and broadest resolutions. A triangular or rectangular distribution with base width τ can be defined and compared using their standard deviations, $\sigma_{\wedge}$ and $\sigma_{\sqcap}$, respectively:[43]

$$\sigma_{\wedge} = \frac{\tau}{\sqrt{(24)}}; \sigma_{\sqcap} = \frac{\tau}{\sqrt{(12)}}. \quad (8)$$

Figure 5(c) shows the variation of the ratio between the standard deviation σ and the base width τ using both analytical calculations and McStas simulations of the time pulse transmitted through a CR double blind chopper pair at the PS position. The pulse shape can therefore be compared across a wide range of wavelengths and energy resolutions for VOR. A PS chopper frequency of 252 Hz, 168 Hz, and 126 Hz for $\Delta E/E = 2.4\%$, 4.2%, and 6.1%, respectively, has been simulated with 1 cm spacing between the members of each CR chopper pair and varying distances, 16 cm, 27 cm, and 38 cm between the CR pairs. The beam profiles vary between the triangular distribution for low wavelengths and extend to an almost rectangular distribution for high wavelengths. For identical standard deviations, the area under a rectangular distribution is a factor of $\sqrt{(2)}$ greater than the area under triangular distribution. It is therefore preferential to obtain a rectangular distribution, more readily obtained with CR choppers. The requirement for CR choppers is thus apparent. The analytical calculations do not account for the time width of the moderator pulse. This is manifested as a general underestimation of the transmission curve standard deviations relative to the simulated results. To emphasize this point, Figure 6 compares one calculated and one simulated transmission curve with the 2nd axis on a logarithmic scale. The fastest and slowest neutrons that pass through the first chopper set will extend the pulse in time up to the second chopper set. The transmitted neutrons therefore develop tails that are not accounted for in the analytical model and become more prominent with increased chopper distances Z, thereby further extending the offset between analytical and simulated data. The impact of the finite time width of the moderator pulse is detailed further in Sec. V A. Figure 7 shows 13 pulses transmitted by the RC PS choppers in a single ESS period using analytical considerations with McStas simulations superposed. The average

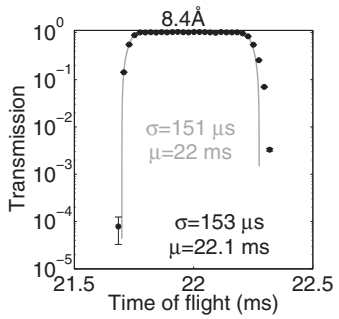

FIG. 6. A comparison of the simulated and calculated transmission curve for the RC PS chopper system. The simulated transmission is shown as data points while the full curve indicates the analytically calculated transmission. The neutron wavelength is 8.4 Å, the chopper frequency is 168 Hz and the CR pairs are separated by the distance 27 cm.

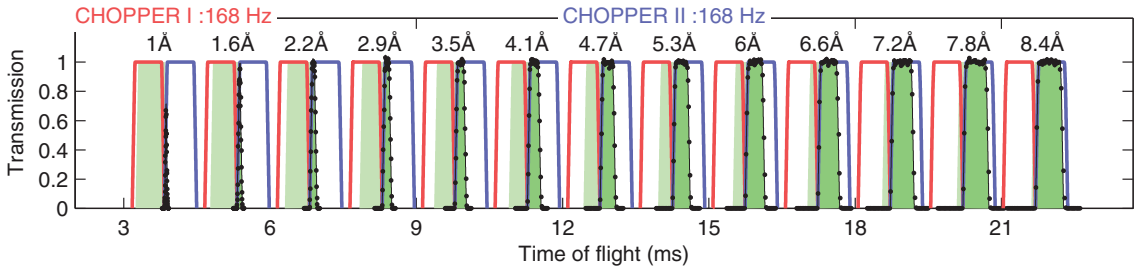

FIG. 7. Thirteen pulses transmitted by the RC PS choppers using analytical considerations, continuous lines, with McStas simulations superposed, dotted line. The dark green sections are the time pulses transmitted through the two sets of PS CR choppers.

relative energy resolution of this set up is 4.2%. The neutron wavelength dependence of the time pulse and the variation of the peak shape from triangular to rectangular are nicely exemplified.

The flux profiles on the sample depend on the transmission of the peak source brightness through the PS and M choppers. Figures 8(a) and 8(b) show the wavelength dependence of the transmission, relative to peak transmission, for a range of energy resolutions. The frequency of the PS chopper depends on $\Delta E/E$ with a rotation frequency of 252 Hz, 168 Hz, and 126 Hz for $\Delta E/E = 2.4\%$, 4.2%, and 6.1%. Above 1.5 Å the peak transmission is greater than 80% for all energy resolutions displayed. Rotating the PS choppers at higher frequencies, up to 336 Hz, results in tighter energy resolutions with better transmission at the lowest wavelengths but at the expense of a slightly non-uniform $\Delta E/E$ at the highest wavelengths. Figure 8(b) shows the transmission for the M chopper set with the M choppers rotating at 336 Hz. The transmission is greater than 80% for wavelengths above 3 Å and $\Delta E/E = 2.4\%$, while for the broader energy resolutions a transmission greater than 80% is reached at 1.5 Å. Clearly higher chopper frequencies will improve these transmission profiles.

A. RC configuration: Energy resolution

The elastic energy resolutions are calculated using analytical considerations and compared to McStas simulations. Figure 9(a) shows typical examples of the wavelength dependence of the elastic energy resolution. The energy resolution, $\Delta E/E$ (FWHM), across the wavelength bandwidth is almost uniform. The peak shape variation of the time pulses, from triangular to rectangular, across the wavelength range has a small impact on the energy resolution and produces a variation of approximately 20% across the full wavelength band. There is a small offset between analytical calculations and simulations due to the time width of the neutron time pulse, an issue which was discussed in relation to Figure 6. Figure 9(b) shows the elastic scattering from the simulated Vanadium sample into the detector for a range of incident wavelengths and energy resolutions, $\Delta E/E$. The line shapes are nicely symmetric in energy and this will enable a generic function to be used to fit the line shapes, although this has not yet been achieved.

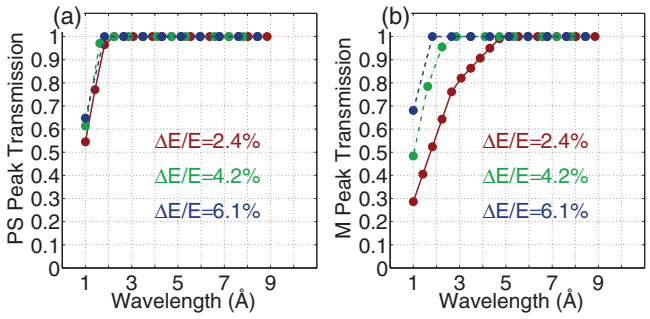

FIG. 8. The peak transmission of the VOR PS (a) and M (b) choppers as function of wavelength for 3 different energy resolutions.

B. RC configuration: Flux at the sample

Figure 10 shows the wavelength dependence of the expected flux on a 1 × 1 cm^2 sample area for a single incident

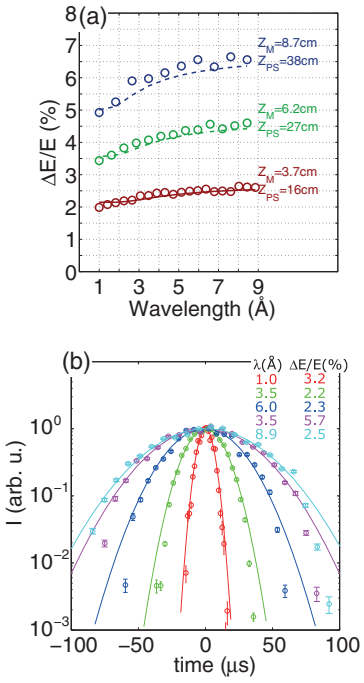

FIG. 9. (a) Wavelength dependence of $\Delta E/E$ for 3 different chopper configurations, assuming a cylindrical sample with diameter 1 cm and height 1 cm. The data points are simulated results, the lines are calculated from the guide dimensions, chopper blade geometry and chopper spacing. (b) McStas simulated time of flight line shapes of elastic scattering from a vanadium scatterer for a range of incident wavelengths and energy resolutions. The lines are simple Gaussian fits to the data. At low intensities the Gaussian profile does not fit the data. However, the fitted curves indicate that the profiles are symmetric and a different generic function may be found to fit the data.

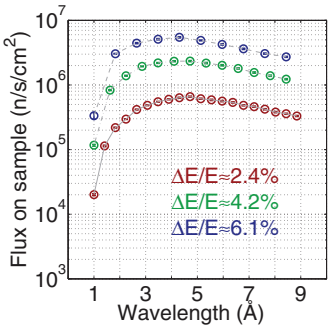

FIG. 10. Flux (ns^{-1} cm^{-2}) at the sample area for a range of wavelengths and energy resolutions using the RC chopper configuration.

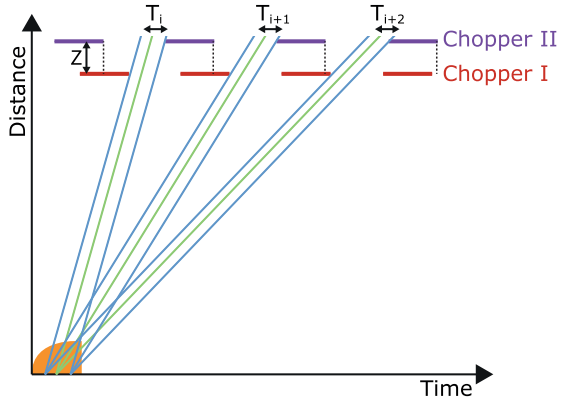

FIG. 11. Time distance diagram that explains the transmission of the PS chopper set for constant opening times across the source period. The orange shape represents the moderator pulse structure.

wavelength with the energy resolution proposed using the RC chopper configuration outlined. Several energy resolutions are proposed but it should be noted that these can be varied continuously and will not be discrete.

VI. RELATIVE VARIABLE ENERGY RESOLUTION

Direct geometry neutron spectrometers provide time scales and scattering profiles that are ideal to probe relaxational behaviour. A few examples include soft matter, biological systems, and energy materials. In the dynamics of molecular liquids a broad range of time scales are covered, ranging from the fast local relaxation of the atomic bonds to global motions of a whole chain. The dynamics occurring on time scales in-between are even more complex due to the interplay of intra- and intermolecular interactions.[44] In order to ascertain all interactions that drive these behaviours it is important to access a broad range of time scales, from ps to ms.[44] In order to vary the elastic energy resolutions on a reactor source, the choppers are rephased between each measurement with considerable time expense. On a current day spallation source direct geometry spectrometer, a broad range of energy resolutions are probed via the use of RRM within a single source period. It will be beneficial for the chopper system outlined in the RC section to also provide such a broad range of energy resolutions. However, the large windows in the chopper blades do not lend themselves to providing energy resolutions as low as 10 μeV using a simple counter rotating chopper pair. It is nevertheless possible to access a broad range of energy resolutions using two different configurations for the PS and M choppers. These configurations, outlined in Secs. VI A and VI B, are able to provide three to four orders of magnitude in time, necessary to probe complex relaxational behaviour.

A. RV configuration: PS choppers for constant opening times

Figure 11 shows a time distance diagram that explains how a constant opening time is achieved at the PS choppers in the RV configuration. Two choppers separated by a distance Z, up to 38 cm, rotate at different frequencies $F_{\mathrm{I}} > F_{\mathrm{II}}$, both an integer multiple of the ESS source. The opening times $\mathrm{T}_i \rightarrow \mathrm{T}_{i+2}$ are provided by the closing edge of the slower rotating chopper and the opening edge of the faster rotating chopper. Similar to the RC chopper configuration it is important to provide well defined opening times, only possible using counter rotating choppers. Choppers I and II in Figure 11 are therefore CR pairs. The resultant calculated and simulated time dependent transmission of neutrons through the PS choppers is shown in Figure 12.

The red and blue curves indicate the pulses transmitted by choppers I and II, respectively. The green areas show the arrival of the pulses from chopper I at chopper II, and the pulses transmitted by the complete system is the overlap between the green areas and the blue curves, the darker green areas. The base widths τ is related to the times of the opening and closing of choppers I and II, $T_{\mathrm{closeII,\,0}}$ and $T_{\mathrm{openI,\,0}}$, respectively, as

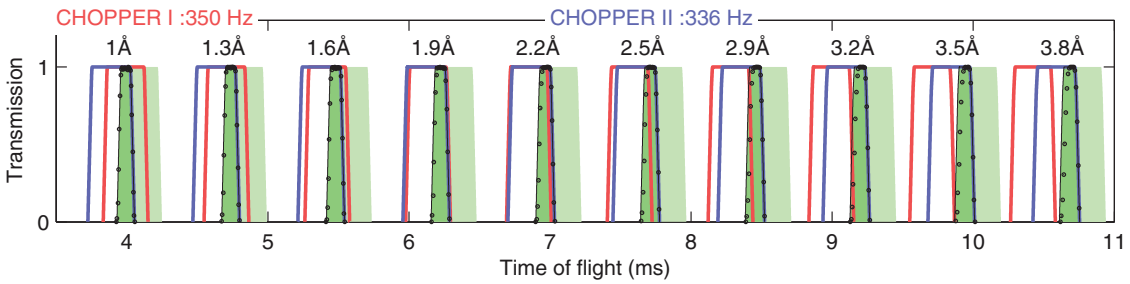

FIG. 12. Time dependent transmission of the PS choppers. Blue and red lines are the opening of choppers I and II, respectively. The light green block is the neutron flux just before it reaches chopper II in time in Figure 11. The dark green area represents the time opening of the complete PS chopper set. The black dots represent McStas simulated result.

follows:

$$\tau_i = \left(T_{\text{close II},0} + \frac{i}{F_{\text{II}}}\right) - \left(T_{\text{open I},0} + \frac{i}{F_{\text{I}}} + \frac{m_n}{h}\lambda_i Z\right), \tag{9}$$

where the wavelength of the first pulse ($i = 0$) is λ_0 and the subsequent pulses have wavelengths $\lambda_i = \lambda_0 + i\delta\lambda$. $\delta\lambda = (F\frac{m_n}{h}(L0 - L1))^{-1}$ is determined by the distances L0 and L1, as defined in Figure 1, and chopper frequency. To achieve identical base widths across the whole wavelength band, Z and the frequencies of the chopper pairs I and II are tuned according to

$$\frac{1}{F_{\text{II}}} - \frac{1}{F_{\text{I}}} = \frac{m_n}{h}\delta\lambda Z\,, \tag{10}$$

which reduces Eq. (9) to

$$\tau = T_{\text{close II},0} - T_{\text{open I},0} - \frac{m_n}{h}\lambda_0 Z \tag{11}$$

and the dependency of the base widths τ on the individual wavelengths λ_i vanishes. In the VOR RV configuration we have $F_{\text{I}} = 350$ Hz and $F_{\text{II}} = 336$ Hz corresponding to $\delta\lambda \approx 1.2$ Å and Z = 38.8 cm. There are 4 slits in each PS chopper, see Table I, and therefore pulses are transmitted with a constant variation of $\delta\lambda \approx 0.3$ Å. Figure 12 shows 10 of the 30 pulses of the VOR usable bandwidth in the RV PS chopper configuration comparing the analytical calculations to the McStas simulations. There are two points to note. First, the time opening is equivalent for all incident wavelengths. Second, the transmission is unity for all incident wavelengths.

B. RV configuration: M choppers for constant opening times

The very short opening times and the limited maximum distance between the chopper pair at the M chopper position, $Z_{\max} = 10$ cm, make it impossible to employ the method outlined for the PS choppers to achieve a constant burst time across the source period. Instead, the M choppers are phased in a similar manner to the M choppers of the RC mode both rotating at 336 Hz, with a slight offset in time so that chopper II opens slightly before chopper I closes. To suppress the wavelength dependency of the burst times, the 2 sets of counter rotating choppers are employed with 2 cm between the chopper pair centers. Figure 13 shows the time dependent transmission of the M choppers. The green area shows the neutron transmission through the first set of choppers while the dark green region represents the transmission through the complete M chopper set. The transmission through the PS chopper set has been considered and is reflected by the fact that only one in three opening times transmit pulses. This is due to the physical position of the PS and M choppers, x:3x with x = 9.5 m on VOR.

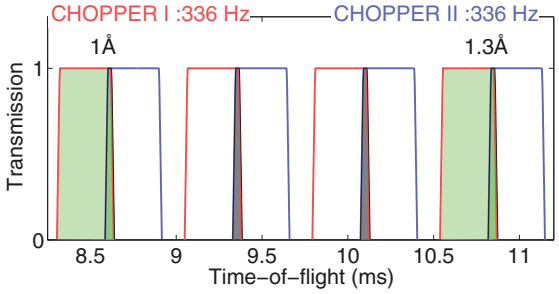

FIG. 13. Cartoon that shows the time dependent transmission of the M choppers. Light green shows the neutron transmission through the first set of choppers while the dark green region represents the transmission through the complete M chopper set.

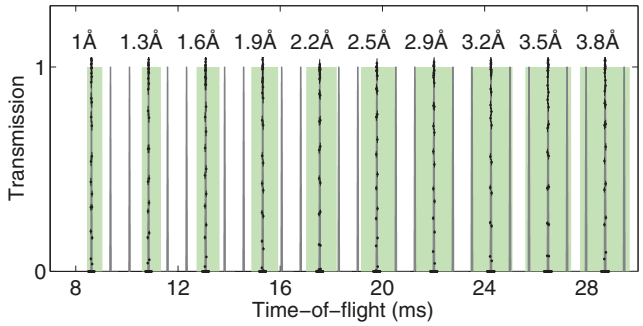

FIG. 14. The time width of the PS chopper neutron pulses extend between the PS and M choppers. The green blocks represent the time spread of a few incident wavelengths at the M chopper. The continuous grey lines represent the analytical opening times of the M chopper set and the black dotted lines represent the McStas simulated wavelengths extracted.

The precise behaviour of the opening times of the M choppers with respect to the pulses transmitted through the PS choppers is displayed in Figure 14 with the green blocks representing the time spread of the various incident wavelengths from the PS to the M choppers, the grey continuous lines are the analytical opening times of the M chopper set with the dotted lines the McStas simulations of the pulses extracted from the M choppers. Further choppers are envisaged to suppress unwanted pulses if required, see Table I.

The resultant opening times for both the M and PS choppers are presented in Figure 15(a) for different ΔE/E ranges. The dotted lines represent McStas simulations while the continuous lines are analytical calculations. There is less correspondence between simulation and analytical calculation as the opening times are extended for the higher energy resolutions. This is a consequence of the extended wavelength band transmitted with wide opening times resulting in longer tails of the neutron transmission profiles. It is clear that the

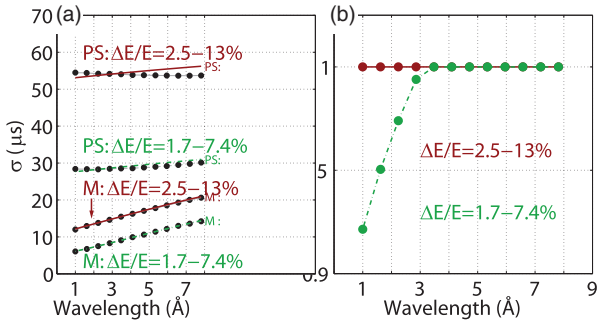

FIG. 15. (a) Wavelength dependence of the opening times for the PS and M choppers for different ranges of energy resolutions. Continuous lines are analytical calculations and dotted lines are the McStas simulations. (b) Wavelength dependence of the transmission through the M chopper set for two energy ranges.

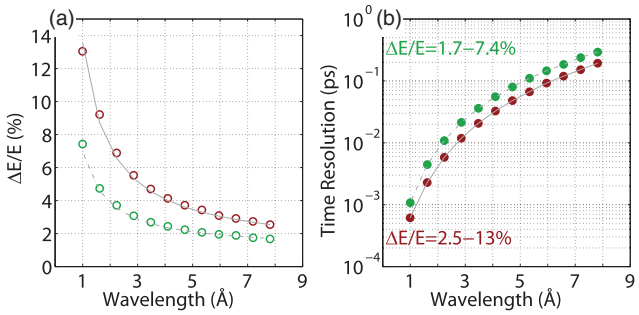

FIG. 16. (a) Energy resolutions, ΔE/E, probed in a single source period of the relative variable energy configuration. (b) Corresponding time resolutions.

wavelength dependence of the M chopper opening times in RV mode is less uniform than the PS opening times. However, the variation is not so great and allows the required range in energy resolutions to be accessed across the ESS source period.

The wavelength dependence of the transmission through the M chopper set is presented in Figure 15(b) for two different ranges of energy resolutions as provided by varying the offset time. The more relaxed energy resolutions, 2.5%–13%, provide a unity peak transmission for all wavelengths while the energy range $\Delta E/E = 1.7\%–7.4\%$ shows a slight loss of transmission for $\lambda < 3$ Å from unity to 90%.

C. RV configuration: Energy and time resolution

The resultant energy resolutions probed in a single source period of the RV energy configuration are shown Figure 16(a) for the two settings, 1.7%–7.4% and 2.5%–13%. The corresponding time resolutions accessed in a single source period are shown in Figure 16(b). Three orders of magnitude can be accessed with full transmission through both PS and M choppers. This can be extended in time at the smallest time resolutions when the transmitted neutron pulses with reduced transmissions are included. Figure 17 shows the wavelength dependence of the simulated flux on a 1×1 cm^2 sample area for each single incident wavelength with the energy bands proposed using the RV chopper configuration.

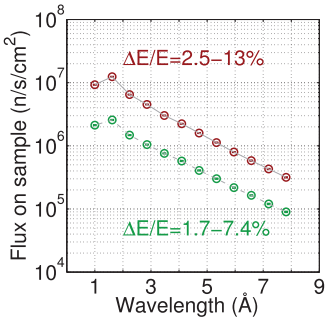

FIG. 17. The wavelength dependence of the simulated flux on a 1×1 cm^2 sample area for each single incident wavelength with the energy bands proposed using the RV chopper configuration outlined.

VII. CONCLUSION

A novel chopper concept is proposed for neutron direct geometry spectrometers that will optimise the use of RRM. Two configurations are presented. First, the RC configuration provides a constant relative energy resolution across the bandwidth thus providing a more uniform flux profile for all the incident wavelengths. Accessing broad regions of S(**Q**, ω) will be possible and thus rapidly ascertain the scattering profiles of novel materials. In conjunction with the increased brightness of the ESS the possibility to probe materials that are currently inaccessible due to weak scattering profiles, as a result of either restricted sample growth and/or weaker scattering signals, can be realised. Most importantly, probing the time dependence of transient phenomena with a broad range of excitations will become standard.

Second, the RV chopper configuration provides a broad range of time windows via the widely varied energy resolutions through the use of RRM across the full wavelength bandwidth. Access to a broad range of time windows is crucial for the multiscale discipline of soft matter in which complexity is revealed via a large number of relaxational phenomena on different time scales. The ability to probe these time scales in a single shot is greatly beneficial for sample dependent and lifetime limited samples. These novel chopper concepts incorporate an important innovation that will bring the entire field of neutron scattering forward.[45]

ACKNOWLEDGMENTS

The support from and useful discussions with the Scientific and Technical Advisory Panel (STAP) for Direct Geometry Spectroscopy of the ESS is gratefully acknowledged.

[1]R. Bewley and R. Eccleston, Nucl. Instrum. Methods Phys. Res., Sect. A **492**, 97 (2002).
[2]M. B. Stone, J. L. Niedziela, D. L. Abernathy, L. deBeer Schmitt, G. Ehlers, O. Garlea, G. E. Granroth, M. Graves-Brookes, A. I. Kolesnikov, A. Podlesnyak, and B. Winn, Rev. Sci. Instrum. **85**, 045113 (2014).
[3]G. Ehlers, A. A. Podlesnyak, J. L. Niedziela, E. B. Iverson, and P. E. Sokol, Rev. Sci. Instrum. **82**, 085108 (2011).
[4]J. Ollivier and J.-M. Zanotti, Collect. SFN **10**, 379 (2010).
[5]R. Kajimoto, M. Nakamura, Y. Inamura, F. Mizuno, S. O.-K. K. Nakajima, T. Yokoo, T. Nakatani, R. Maruyama, K. Soyama, K. Shibata, K. Suzuya, S. Sato, K. Aizawa, M. Arai, S. Wakimoto, M. Ishikado, S. Shamoto, M. Fujita, H. Hiraka, K. Ohoyama, K. Yamada, and C.-H. Lee, J. Phys. Soc. Jpn. **80**, SB025 (2010).
[6]K. Nakajima, S. Ohira-Kawamura, T. Kikuchi, M. Nakamura, R. Kajimoto, Y. Inamura, N. T. andd K. Aizawa, K. Suzuya, K. Shibata, T. Nakatani, K. Soyama, R. Maruyama, H. Tanaka, W. Kambara, T. Iwahashi, Y. Itoh, T. Osakabe, S. Wakimoto, K. Kakurai, F. Maekawa, M. Harada, K. Oikawa, R. E. Lechner, F. Mezei, and M. Arai, J. Phys. Soc. Jpn. **80**, SB028 (2011).
[7]See http://www.helmholtz-berlin.de/forschung/oe/em/soft-matter/forschung/laufzeit/spectrometer-neat_en.html for the official homepage of the Time-Of-Flight Spectrometer NEAT.
[8]See http://www.ncnr.nist.gov/instruments/dcs/ for the official homepage of the NCNR Disk Chopper Spectrometer (DCS).
[9]See http://www-llb.cea.fr/spectros/pdf/mibemol-llb.pdf for the official homepage of the Inelastic time-of-flight Spectrometer MIBEMOL.
[10]See http://www.ansto.gov.au/ResearchHub/Bragg/Facilities/Instruments/Pelican/ for the official homepage of Pelican time-of-flight Spectrometer.
[11]J.-Y. So, M. Moon, S.-J. Cho, Y.-H. Choi, C.-H. Lee, and J.-G. Park, J. Neutron Res. **15**, 23 (2007).

[12]F. Mezei, M. Russina, and S. Schorr, Physica B **276–278**, 128 (2000).
[13]M. Russina and F. Mezei, Proc. SPIE **4785**, 24–33 (2002).
[14]M. Russina and F. Mezei, Nucl. Instrum. Methods Phys. Res., Sect. A **604**, 624 (2009).
[15]M. Russina and F. Mezei, J. Phys.: Conf. Ser. **251**, 012079 (2010).
[16]C. Windsor, *Pulsed Neutron Scattering* (Taylor & Francis, 1981).
[17]C. J. Carlisle, A. D. Taylor, and W. G. Williams, in *Proceeding of the International Conference on Neutron Scattering in the 90s* (IAEA, 1985), Chap. CN-46/8P, pp. 421–434.
[18]R. E. Lechner, in Proceedings of the ICANS-XI, KEK Reports 90-25 (1991).
[19]P. P. Deen, A. Vickery, A. K. H, and R. Hall-Wilton, "A design study of VOR: a versatile optimal resolution chopper spectrometer for the ESS," Eur. Phys. J. (submitted).
[20]P. Willendrup, E. Farhi, E. Bergbäck Knudsen, U. Filges, and K. Lefmann, J. Neutron Res. **17**, 35 (2014).
[21]See http://www.ill.eu/instruments-support/instruments-groups/instruments/in5/characteristics/ for characteristics of the ILL instruments.
[22]See http://www.isis.stfc.ac.uk/instruments/let/technical/let-technical-information6998.html for technical information about the cold neutron multi-chopper spectrometer LET at ISIS.
[23]See http://neutrons.ornl.gov/cncs/specifications/ for the specifications of the Cold Neutron Chopper Spectrometer (CNCS) at SNS.
[24]J. Copley, Nucl. Instrum. Methods Phys. Res., Sec. A **291**, 519 (1990).
[25]K. Lefmann and K. Nielsen, Neutron News **10**, 20 (1999).
[26]D. Wechsler, G. Zsigmond, F. Streffer, and F. Mezei, Neutron News **11**, 25 (2000).
[27]K. Lieutenant, G. Zsigmond, S. Manoshin, M. Fromme, H. N. Bordallo, D. Champion, J. Peters, and F. Mezei, "Neutron instrument simulation and optimization using the software package vitess," Proc. SPIE **5536**, 134–145 (2004).
[28]H. Arima, K. Komatsu, K. Ikeda, K. Hirota, and H. Kagi, Nucl. Instrum. Methods Phys. Res., Sect. A **600**, 71 (2009).
[29]R. Kajimoto, K. Nakajima, M. Nakamura, K. Soyama, T. Yokoo, K. Oikawa, and M. Arai, Nucl. Instrum. Methods Phys. Res., Sect. A **600**, 185 (2009).
[30]G. Granroth, D. Vandergriff, and S. Nagler, Physica B **385–386**(Part 2), 1104 (2006). Proceedings of the Eighth International Conference on Neutron Scattering.
[31]Z. Izaola and M. Russina, J. Phys.: Conf. Ser. **251**, 012064 (2010).
[32]H. Arima, T. Hattori, K. Komatsu, J. Abe, W. Utsumi, H. Kagi, A. Suzuki, K. Suzuya, T. Kamiyama, M. Arai, and T. Yagi, J. Phys.: Conf. Ser. **215**, 012025 (2010).
[33]P. Freeman, H. M. Rønnow, C. Niedermayer, F. Jurnyi, M. Mark, K. Lefmann, J. O. Birk, M. Bertelsen, N. B. Christensen, and J. Larsen, "ESS instrument construction proposal CAMEA," Technical Report, 2014; this work is carried out as part of the CAMEA work project. Members of this project are: Paul G. Freeman, Henrik M. Ronnow (EPFL), Christof Niedermayer, Fanni Jurányi, Márton Markó (PSI), Kim Lefmann, Jonas Okkels Birk, Mads Bertelsen (University of Copenhagen), Niels Bech Christensen, Jacob Larsen (Technical University of Denmark).
[34]J. Y. Y. Lin, A. A. Aczel, D. L. Abernathy, S. E. Nagler, W. J. L. Buyers, and G. E. Granroth, Phys. Rev. B **89**, 144302 (2014).
[35]L. Udby, P. K. Willendrup, E. Knudsen, C. Niedermayer, U. Filges, N. B. Christensen, E. Farhi, B. O. Wells, and K. Lefmann, Nucl. Instrum. Methods Phys. Res., Sect. A **634**, S138 (2011). Proceedings of the International Workshop on Neutron Optics {NOP2010}.
[36]E. Farhi, V. Hugouvieux, M. Johnson, and W. Kob, J. Comput. Phys. **228**, 5251 (2009).
[37]E. Farhi, Y. Debab, and P. Willendrup, J. Neutron Res. **17**, 5–18 (2014).
[38]J. Carpenter and D. Mildner, Nucl. Instrum. Methods Phys. Res., Sect. A **301**, 315 (1991).
[39]J. Copley, Nucl. Instrum. Methods Phys. Res., Sect. A **303**, 332 (1991).
[40]A. van Well, Physica B **180–181**(Part 2), 959 (1992).
[41]R. Cubitt and G. Fragneto, Appl. Phys. A **74**, s329 (2002).
[42]M. Strobl, R. Steitz, M. Kreuzer, M. Rose, H. Herrlich, F. Mezei, M. Grunze, and R. Dahint, Rev. Sci. Instrum. **82**, 055101 (2011).
[43]See http://www.itl.nist.gov/div898/handbook/mpc/section5/mpc541.htm for standard deviations from assumed distributions.
[44]H. Morhenn, S. Busch, H. Meyer, D. Richter, W. Petry, and T. Unruh, Phys. Rev. Lett. **111**, 173003 (2013).
[45]T. Unruh, H. Mutka, J. R. Stewart, R. Bewley, M. Koza, R. Kajimoto, and G. Ehlers, ESS STAP Report, 2014.